Understanding the optical anisotropy of oxidized Si(001) surfaces

F. Fuchs, W. G. Schmidt, and F. Bechstedt
Institut für Festkörpertheorie und -optik, Friedrich-Schiller-Universität, Max-Wien-Platz 1, 07743 Jena, Germany
(Received 25 April 2005; revised manuscript received 27 May 2005; published 23 August 2005)

First-principles optical-response calculations of oxidized and strained Si structures are presented. Local Si lattice deformations accompanying the oxidation of Si bulk bonds cause pronounced optical anisotropies that account very well for the reflectance difference signal measured during oxide growth [Yasuda *et al.*, Phys. Rev. Lett. **87**, 037403 (2001)]. In contrast, calculations for various energetically favored (4×2) and (2×2) reconstructed overlayer structures fail to reproduce the experiment.

DOI: 10.1103/PhysRevB.72.075353 PACS number(s): 78.68.+m, 78.66.Db, 81.65.Mq

I. INTRODUCTION

Si oxidation is one of the most interesting and intensively studied subjects of surface physics, but still not completely understood.[1] Mainly photoemission spectroscopy and electron diffraction have been used to explore the oxidation process. The penetration depth of electrons limits these techniques to the monitoring of the uppermost few monolayers. Photons, on the other hand, penetrate deeply into the substrate, of the order of 10^3 Å. Optical spectroscopies such as reflectance difference/anisotropy spectroscopy (RDS/RAS) should thus be helpful to explore and monitor the microscopic processes during the oxidation, even far below the surface. RDS spectra measured during thermal oxide growth on single-domain Si(001) surfaces[2–4] show oscillations, i.e., repeated changes of the optical anisotropy polarity, for photon energies around the E_1 and E_2 critical points (CPs) of bulk Si as well as above 5 eV. Scanning reflection electron microscopy[5] and total-energy calculations[6] indicate that the thermal oxidation of Si(001) proceeds layer-by-layer. This suggests to relate the RDS oscillations to the Si layer oxidation. If the relation between the RDS oscillations and the microscopic details of the oxide growth was understood, optical spectroscopy with all its advantages of *in situ* applicability could be used to investigate and quantitatively monitor the oxidation process, including oxide thickness measurements with atomic resolution. However, neither the experiments[2–4] nor previous numerical simulations[7–9] succeeded in explaining convincingly how the microscopic oxidation phenomena manifest themselves in the RDS data.

The present work aims at explaining the physics behind the oxidation-induced RDS oscillations. Total-energy and optical-response calculations are performed for a large number of oxidized Si(001) surface and bulk structures. The computational results indicate that it is the progression of the Si deformation pattern underneath the disordered silicon oxide film that causes the measured RDS oscillations. These show a one-to-one correspondence with the monolayer oxidation.

II. METHODOLOGY

The calculations are performed using the Vienna *ab initio* simulation package (VASP) implementation[10] of the gradient-corrected[11] density functional theory (DFT-GGA). The electron-ion interaction is described by the projector augmented-wave (PAW) method.[12,13] We expand the valence wave functions into plane waves up to an energy cutoff of 30 Ry. The Si(001) surface is modeled with symmetric, periodically repeated supercells consisting of 12 atomic Si layers including oxidized layers and a vacuum region equivalent in thickness to eight atomic layers. Sets corresponding to 64 and 256 **k** points in the full (1×1) surface Brillouin zone are used to calculate the ground-state electronic structure and the optical response, respectively. In order to avoid an artificial bias due to the **k**-point set for the calculation of the strained Si sample, we employed 200 000 random points in this case. The reflectance anisotropy is calculated according to the scheme devised by Del Sole[14,15]

$$\frac{\Delta r_i}{r}(\omega)=\frac{8\omega\pi}{c}\,\mathrm{Im}\left\{\frac{\alpha_{ii}^{hs}(\omega)}{\epsilon_b(\omega)-1}\right\}, \tag{1}$$

where the slab polarizability α and the bulk dielectric function ϵ_b are obtained in independent-particle approximation, i.e., neglecting excitonic and local-field effects.[16]

In order to actually compute the polarizability, momentum matrix elements $\mathbf{p}_{NM}=\langle\Psi_N|\hat{\mathbf{p}}|\Psi_M\rangle$ between Mth and Nth electron state need to be calculated. In the PAW method the all-electron wave functions Ψ_N are related to pseudo-wave functions $\tilde{\Psi}_N$ by means of the linear transformation[12,13]

$$|\Psi_N\rangle=|\tilde{\Psi}_N\rangle+\sum_i\left(|\psi_i\rangle-|\tilde{\psi}_i\rangle\right)\langle\tilde{p}_i|\tilde{\Psi}_N\rangle, \tag{2}$$

where the index i denotes atomic site, the angular momentum quantum number and the reference energy of the all-electron and pseudo atomic partial waves ψ_i and $\tilde{\psi}_i$. The projectors $\tilde{p}_i$ are dual to the pseudo partial waves. Accordingly, we calculate the momentum matrix elements using the expression[17,18]

$$\mathbf{p}_{NM}=\langle\tilde{\Psi}_N|\hat{\mathbf{p}}|\tilde{\Psi}_M\rangle+\sum_{i,j}\langle\tilde{\Psi}_N|\tilde{p}_i\rangle\left(\langle\psi_i|\hat{\mathbf{p}}|\psi_j\rangle-\langle\tilde{\psi}_i|\hat{\mathbf{p}}|\tilde{\psi}_j\rangle\right)\langle\tilde{p}_j|\tilde{\Psi}_M\rangle. \tag{3}$$

The scissors operator[19] with an energy shift of 0.5 eV is used to account for the band-gap underestimation in DFT. RDS spectra are difference spectra, which are furthermore

 ©2005 The American Physical Society

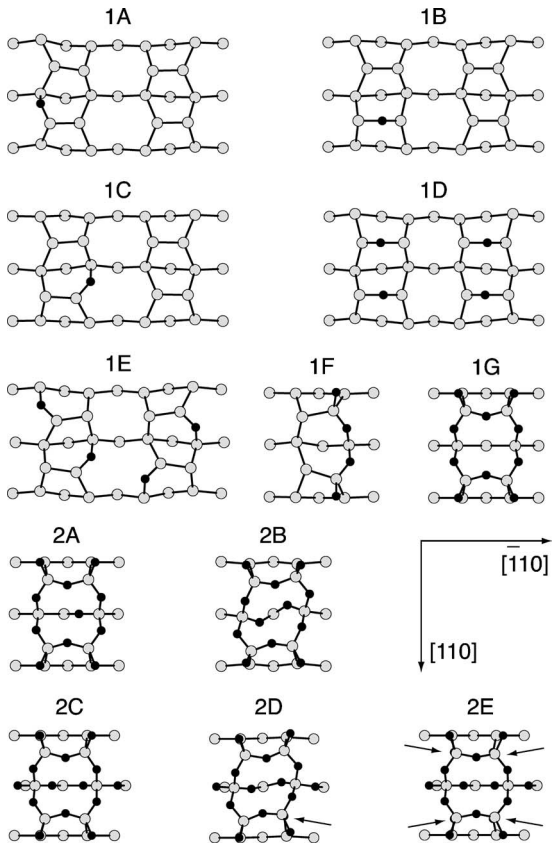

FIG. 1. Top view of the models used to describe oxidation of the first ($1A-1G$) and the uppermost two Si(001) layers ($2A-2E$). Dark and grey symbols indicate O and Si atoms, respectively. Small arrows indicate O atoms hidden below Si atoms.

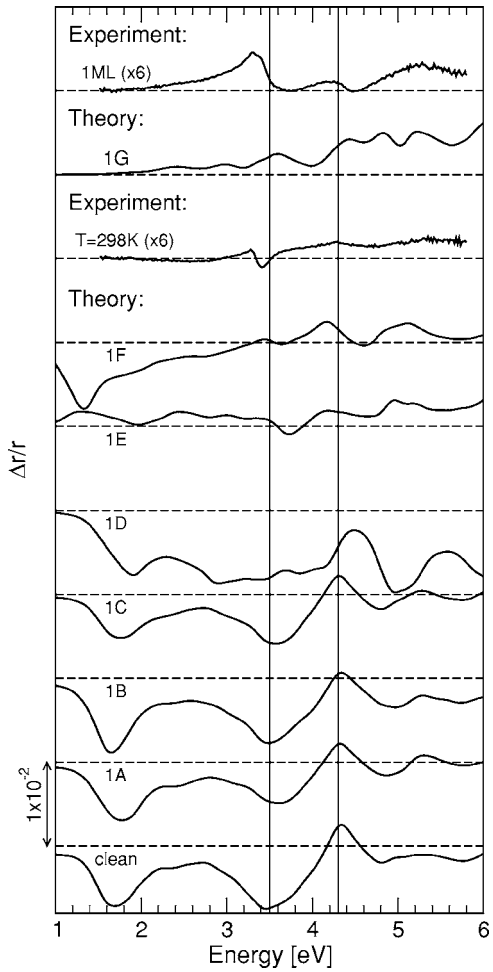

FIG. 2. RDS spectra $[\mathrm{Re}\{(r_{[\bar{1}10]}-r_{[110]})/\langle r\rangle\}]$ calculated for the oxidized Si(001) configurations shown in Fig. 1 are compared with results for the clean surface and measured data from Ref. 2. The calculated positions of the E_1 and E_2 energies are indicated.

normalized to the bulk dielectric function [Eq. (1)]. Therefore, calculations within the independent-particle approximation reliably reproduce experimental data for a wide range of semiconductors.[20,21]

Extensive tests on the slab dimensions, the number of **k** points and the basis set size were performed to ascertain the numerical reliability of our calculations.[22]

III. RESULTS AND DISCUSSION

To model the initial stage of Si(001) surface oxidation, we consider energetically favored surface structures (cf. Fig. 1) where oxidation occurs in the uppermost and the second Si surface layer. For these structures we determine adsorption energies with respect to spin-triplet atomic oxygen that are very close to the values predicted in Ref. 23. To be specific, the adsorption energies per oxygen atom obtained here are always 0.1–0.2 eV lower than those calculated by Yamasaki *et al.*[23]

The calculated RDS spectra of the structures used to model the oxidation of the upper-most atomic layer together with our results for the clean Si(001)$c(4\times2)$ surface are shown in Fig. 2. The optical anisotropy of the clean surface shows a strong, dimer-state related minimum for photon energies of 1.7 eV.[4,24] The measured spectra for oxidized Si(001) show little anisotropy for energies below 2.5 eV.[2] The 1.7 eV feature is quenched, due to the saturation of the Si-dimer states. Submonolayer oxidation at room temperature leads to an overall positive anisotropy signal, apart from a small negative feature near the E_1 CP (cf. 298 K spectrum in Fig. 2). Of all the low-coverage structures considered here, i.e., models $1A$-$1F$, only models $1E$ and $1F$ show a remotely similar feature in the calculated RDS.

Oxidation at about 1000 K for 8 s changes the measured spectrum, giving rise to positive anisotropies for all photon energies considered, with maxima close to the E_1 and E_2 CPs and at about 5.3 eV (cf. uppermost curve in Fig. 2). Yasuda *et al.*[2] assigned this spectrum to the complete oxidation of the first atomic monolayer. Of all the structures investigated computationally, only $1G$ gives rise to an optical anisotropy that is positive throughout the photon energy range probed. The simulated RDS spectra in comparison with experiment thus support earlier findings[25] indicating that the backbonds of the lower Si dimer atom are attacked first by oxygen, before it is inserted into the remaining Si-Si bonds at the surface. However, the deviations in line shape between the calculated spectra and the data measured for room and high temperature oxidation are considerable. Obviously, at no

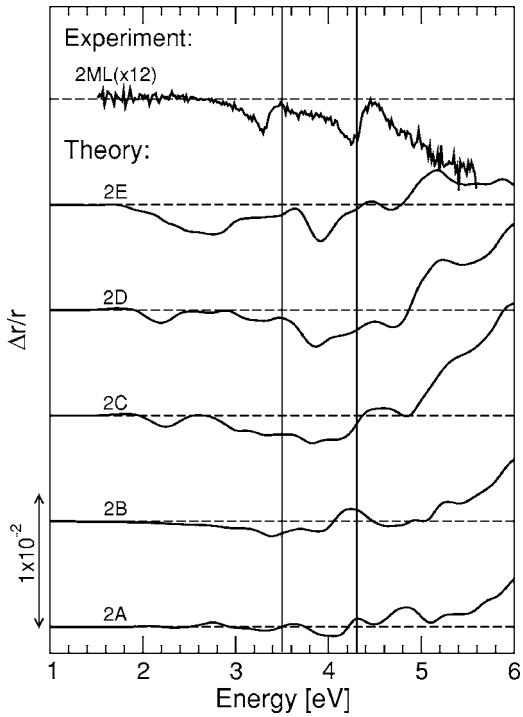

FIG. 3. RDS spectra $[\mathrm{Re}\{(r_{[\bar{1}10]}-r_{[110]})/\langle r\rangle\}]$ calculated for the oxidized Si(001) configurations shown in Fig. 1 are compared with measured data from Ref. 2. The calculated positions of the E_1 and E_2 energies are indicated.

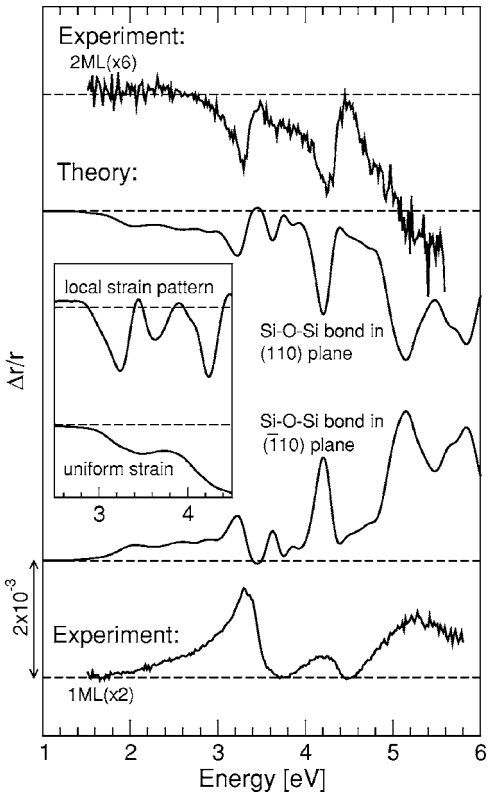

FIG. 4. Calculated optical anisotropy for modified Si bulk structures (see text) in comparison with measured reflectance anisotropy data from Ref. 2.

time during the oxidation the surface is completely ordered with a symmetry corresponding to one of the structural models probed here.

The calculated RDS spectra for models where both the first and the second Si layer are oxidized are compared with the experimental data assigned to the oxidation of the second monolayer[2] in Fig. 3. Experimentally, nearly an inversion of the signal is observed, compared to the spectrum assigned to the oxidation of the first monolayer (this inversion occurs repeatedly during the progression of the oxidation). Negative anisotropies occur for photon energies close to the Si bulk CPs and above 4.5 eV. Clearly, none of the calculated spectra reproduces the overall negative anisotropy, strong deviations from experiment occur in all cases.

High-energy electron diffraction data[5] and scanning tunneling microscopy images of Si(001) surfaces exposed to oxygen[26] indicate that the oxidation causes considerable surface disorder. Therefore, it may be questionable to model the Si surface oxidation with translationally invariant models such as shown in Fig. 1, in particular when optical spectra are simulated that average over a large part of the sample surface. In addition, the repeated oscillations of the RDS signal during Si oxidation seem hardly compatible with an effect originating from ordered surface structures.

Bulk Si is optically isotropic. If the disorder of the oxide film above the interface would render this film optically isotropic too, the only source of optical anisotropy were oxygen atoms inserted into Si-Si bulk bonds directly at the interface. We model this effect by studying the optical anisotropy induced by oxygen inserted into bulk Si bonds. For compatibility with the surface calculations, we use an orthorhombic supercell with $2\times2\times20$ periodicities along the $[\bar{1}10]$, $[110]$, and $[001]$ directions, respectively. (Test calculations with $4\times2\times20$ and $1\times1\times20$ periodicities[22] resulted in similar features as discussed below.) The difference of the calculated $[\bar{1}10]$ and $[110]$ bulk polarizability components is normalized such as to compare with the reflectance anisotropy from Eq. (1). The results are shown in Fig. 4. They show that oxygen inserted into Si-Si bonds in the $(\bar{1}10)$ plane indeed reproduces the features measured after oxidation of the first monolayer, whereas the oxidation of the second monolayer can be modeled by calculations for oxygen inserted into bulk bonds in the (110) plane (the sign change is obvious for symmetry reasons). Given the simplicity of this idealized model, the agreement between calculation and measurement is impressive. Obviously, the measured RDS oscillations can be explained by assuming that (i) the oxidation occurs layer-by-layer and (ii) the silicon oxide directly above the abrupt interface does not contribute substantially to the optical anisotropy. Figure 4 shows that the simple interface model accounts better for the 2 ML experiment than for the 1 ML signal. This indicates the decrease of the RDS contributions from ordered surface structures with increasing oxide thickness.

After having reproduced the experimental data, we analyze the origin of the measured anisotropies in more detail. Yasuda *et al.*[2] pointed out that their data cannot be explained by model calculations using the Si piezo-optic tensor. On the other hand, earlier measurements of the $\mathrm{Si}\text{-}\mathrm{SiO_2}$ interface

optical properties have often been interpreted in terms of strain-induced shifts of the Si bulk CP energies.[27–29] We perform model calculations for four layers of bulk Si uniformly compressed by 2% along $[\bar{1}10]$, a value that roughly accounts for the lattice deformation around an oxygen atom inserted into a Si(001)(2×2) interface unit cell. As seen from the inset of Fig. 4, the optical anisotropy induced by such a macroscopic strain has the same sign and roughly the same magnitude as the measured signal, but does not reproduce the line shape. Therefore, either specific Si-O bond-related electronic states or the perturbation of Si bulk states due to the complicated deformation pattern around the foreign atom must cause the peculiar features around E_1 and E_2. Based on an analysis of the transition matrix elements between pairs of electronic states contributing to the total RAS signal, we can exclude the first possibility: It is not possible to single out a few characteristic states that cause the optical anisotropy. Rather, the optical anisotropies are caused be a multitude of perturbed Si bulk states, i.e., they are intrinsic according to the classification by Aspnes and Studna,[30] see also, e.g., Refs. 20 and 31. This is not surprising, given the large band gap of all polymorphic forms of silicon dioxide.[32] To further corroborate the bulk Si origin of the optical anisotropies we performed calculations for a supercell containing the Si lattice deformation pattern around an inserted oxygen, but replaced the O atom with two H atoms for Si dangling bond termination. Indeed, a line shape is obtained (cf. "local strain pattern" curve in Fig. 4) that shows features that are somewhat similar to the oxygen inserted case. This indicates that strain-perturbed Si bulk wave functions cause the optical anisotropy. However, it is important to account for the local deformation pattern around the defect. An uniform compression such as assumed by Yasuda and co-workers[2] indeed does not explain the measurements. Figure 5 illustrates the complexity of the Si bulk deformation around an oxidized Si bond.

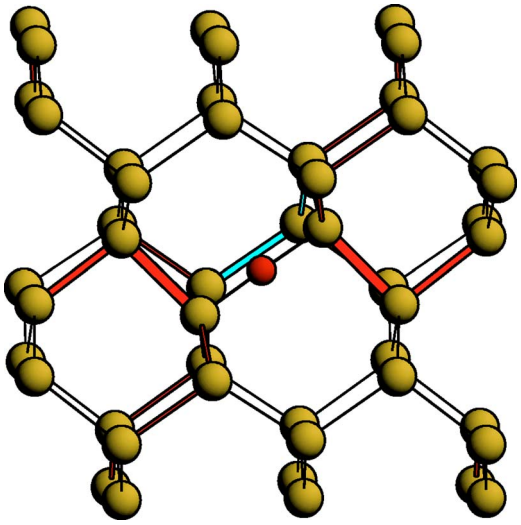

FIG. 5. (Color online) Calculated lattice deformation around an oxidized Si bond within a $2\times2\times20$ supercell. Compressive/tensile strain is indicated by red (dark)/blue (light gray) bonds, with the thickness of the bonds indicating the amount of local strain. The max. value is 2.6%. Large and small symbols indicate Si and O atoms, respectively.

IV. SUMMARY

In conclusion, we calculated the atomic geometries and optical response of a large number of oxidized Si(001) surface structures as well as oxidized and strained silicon bulk systems from first principles. Comparison of the simulated optical spectra with experiment indicates that the oxidation-induced local strain pattern is causing the measured oscillations of the optical anisotropy in one-to-one correspondence to the layer oxidation, while the oxide layers directly above the interface, due to their disorder, contribute relatively little to the optical anisotropy.

ACKNOWLEDGMENTS

We thank Tetsuji Yasuda for suggesting this project and critically reading the manuscript as well as Kaori Seino for numerous discussions. Grants of computer time from the Leibniz-Rechenzentrum München and the Höchstleistungsrechenzentrum Stuttgart are gratefully acknowledged. Financial support was provided by the Deutsche Forschungsgemeinschaft (SCHM-1361/6) and the EU Network of Excellence NANOQUANTA (Contract No. NMP4-CT-2004-500198).

[1] J. Dabrowski and H.-J. Müssig, *Silicon Surfaces and Formation of Interfaces* (World Scientific, Singapore, 2000).
[2] T. Yasuda, S. Yamasaki, M. Nishizawa, N. Miyata, A. Shklyaev, M. Ichikawa, T. Matsudo, and T. Ohta, Phys. Rev. Lett. **87**, 037403 (2001).
[3] T. Yasuda, N. Kumagai, M. Nishizawa, S. Yamasaki, H. Oheda, and K. Yamabe, Phys. Rev. B **67**, 195338 (2003).
[4] T. Yasuda, M. Nishizawa, N. Kumagai, S. Yamasaki, H. Oheda, and K. Yamabe, Thin Solid Films **455–456**, 759 (2004).
[5] H. Watanabe, K. Kato, T. Uda, K. Fujita, M. Ichikawa, T. Kawamura, and K. Terakura, Phys. Rev. Lett. **80**, 345 (1998).
[6] H. Kageshima and K. Shiraishi, Phys. Rev. Lett. **81**, 5936 (1998).
[7] T. Nakayama and M. Murayama, Appl. Phys. Lett. **77**, 4286 (2000).
[8] A. Incze, R. Del Sole, and G. Onida, Phys. Rev. B **71**, 035350 (2005).
[9] W. G. Schmidt, F. Fuchs, A. Hermann, K. Seino, F. Bechstedt, R. Paßmann, M. Wahl, M. Gensch, K. Hinrichs, N. Esser, S. Wang, W. Lu, and J. Bernholc, J. Phys.: Condens. Matter **16**, S4323 (2004).
[10] G. Kresse and J. Furthmüller, Comput. Mater. Sci. **6**, 15 (1996).
[11] J. P. Perdew, J. A. Chevary, S. H. Vosko, K. A. Jackson, M. R.

Pederson, D. J. Singh, and C. Fiolhais, Phys. Rev. B **46**, 6671 (1992).
[12] P. E. Blöchl, Phys. Rev. B **50**, 17953 (1994).
[13] G. Kresse and D. Joubert, Phys. Rev. B **59**, 1758 (1998).
[14] R. Del Sole, Solid State Commun. **37**, 537 (1981).
[15] R. Del Sole and G. Onida, Phys. Rev. B **60**, 5523 (1999).
[16] P. H. Hahn, W. G. Schmidt, and F. Bechstedt, Phys. Rev. Lett. **88**, 016402 (2002).
[17] B. Adolph, J. Furthmüller, and F. Bechstedt, Phys. Rev. B **63**, 125108 (2001).
[18] H. Kageshima and K. Shiraishi, Phys. Rev. B **56**, 14985 (1997).
[19] R. Del Sole and R. Girlanda, Phys. Rev. B **48**, 11789 (1993).
[20] W. G. Schmidt, F. Bechstedt, and J. Bernholc, J. Vac. Sci. Technol. B **18**, 2215 (2000).
[21] W. G. Schmidt, K. Seino, P. Hahn, F. Bechstedt, W. Lu, S. Wang, and J. Bernholc, Thin Solid Films **455/456**, 764 (2004).
[22] F. Fuchs, Master's thesis, Friedrich-Schiller-Universität Jena, 2004.
[23] T. Yamasaki, K. Kato, and T. Uda, Phys. Rev. Lett. **91**, 146102 (2003).
[24] R. Shioda and J. van der Weide, Phys. Rev. B **57**, R6823 (1998).
[25] K. Kato, T. Uda, and K. Terakura, Phys. Rev. Lett. **80**, 2000 (1998).
[26] K. Fujita, H. Watanabe, and M. Ichikawa, Appl. Phys. Lett. **70**, 2807 (1997).
[27] J. T. Fitch, C. H. Bjorkman, G. Lucovsky, F. H. Pollak, and X. Yin, J. Vac. Sci. Technol. B **7**, 775 (1989).
[28] Z. Yang, Y. H. Chen, J. Y. L. Ho, W. K. Liu, X. M. Fang, and P. J. McCann, Appl. Phys. Lett. **71**, 87 (1997).
[29] W. Daum, H.-J. Krause, U. Reichel, and H. Ibach, Phys. Rev. Lett. **71**, 1234 (1993).
[30] D. E. Aspnes and A. A. Studna, Phys. Rev. Lett. **54**, 1956 (1985).
[31] W. G. Schmidt, N. Esser, A. M. Frisch, P. Vogt, J. Bernholc, F. Bechstedt, M. Zorn, T. Hannappel, S. Visbeck, F. Willig, and W. Richter, Phys. Rev. B **61**, R16335 (2000).
[32] Y. N. Xu and W. Y. Ching, Phys. Rev. B **44**, 11048 (1991).